PULLOUT STRENGTH OF NSM CFRP STRIPS BONDED TO VINTAGE CLAY BRICK MASONRY

Dizhur[a] D., Griffith[b] M. C. and Ingham[a] J. M.

[a] *Department of Civil and Environmental Engineering, The University of Auckland, Private Bag 92019, Auckland 1142, New Zealand*

[b] *School of Civil, Environmental and Mining Engineering, The University of Adelaide, Australia*

ABSTRACT

The frequently observed inadequate seismic performance of unreinforced masonry (URM) buildings necessitates the development of cost effective minimally-invasive seismic improvement techniques for this type of construction. One promising solution is use of the near surface mounted (NSM) technique to incorporate fibre reinforced polymers (FRP) strips as longitudinal reinforcement. In particular, the NSM technique provides several advantages over externally bonded (EB) FRP as a seismic improvement technique including significantly higher axial strain at debonding, minimal negative impact upon the aesthetics of the structure, reduced installation time, and superior protection from fire and the environment, thus providing a cost effective and minimally-invasive option for seismically strengthening URM buildings. An experimental program consisting of 39 pull tests was conducted using NSM carbon (C)FRP strips bonded to vintage solid clay brick masonry, to provide data with which to validate the accuracy of existing predictive FRP-to-masonry bond models. Based on experimental findings, a variation of an existing analytical FRP-to-masonry bond model is proposed and the effects of geometric variation of the NSM groove and the reinforcing CFRP strip are discussed.

Keywords:
Historic masonry, clay brick, bond strength, unreinforced masonry (URM), seismic retrofit, near surface mounting (NSM), carbon fibre reinforced polymers (CFRP)

1 BACKGROUND

It is well known and was once again highlighted during the 2010 M7.1 Darfield (New Zealand) earthquake [1] and subsequent 2011 M6.3 aftershock [2], that unreinforced masonry (URM) construction often has insufficient strength to resist lateral earthquake forces in high and moderate seismic zones [3-5]. One of the most critical deficiencies of URM buildings is the lack of wall-diaphragm connections, but once added, it is the out-of-plane bending failure mechanism and subsequent wall collapse that poses the greatest risk to both the building's occupants and to passers-by [6]. To mitigate this risk, various seismic improvement techniques have been developed over the decades. One such established technique for strengthening and increasing the ductility capacity of URM walls subjected to earthquake loading is the use of fibre reinforced polymer (FRP) material. Externally bonded (EB) FRP sheets or plates [7, 8] and, more recently, near-surface mounted (NSM) FRP bars or strips are the two FRP application techniques that are commonly used. Using the NSM strip technique provides several advantages over the EB technique, including significantly higher axial strain at debonding, minimal negative impact upon the aesthetics of the structure, reduced installation time, and superior protection from fire and the environment [9, 10], thus providing a cost effective and minimally-invasive option for seismically strengthening URM buildings. It is typically assumed that a horizontal crack at approximately wall mid-height will initially develop at a low level of out-of-plane loading applied to a vertically-spanning URM wall [11]. Hence, because vertical bending of URM walls is typically critical, the application of vertically oriented strengthening elements to improve the vertical bending capacity of such walls is most appropriate [12].

Accurately predicting the strength of the bond between an NSM FRP strip and the substrate material is essential to ensure the effectiveness of the NSM CFRP strengthening. The intermediate crack (IC) debonding mechanism [13] governs the increase in moment capacity and ductility of structural sections strengthened using NSM FRP, and is considered to be the most critical of the commonly observed debonding mechanisms. A good understanding of FRP-to-concrete bond behaviour and the IC debonding mechanism has been achieved from extensive previous research, as reported by Stone et al. [14] and Hassan and Rizkalla [15], with reliable analytical predictive models for the IC debonding resistance also having being established [16].

Initial experimental validation of the use of NSM FRP as a technique for seismic improvement

of masonry focused on strengthening modern URM and involved simulation of the IC debonding failure mechanism using simple monotonic pull tests [9, 17-19]. The observed failure modes are categorised as: (i) IC debonding failure, where cracking propagated in the masonry; (ii) Sliding failure, where failure occurred at the CFRP strip-adhesive interface; (iii) Rupture of the CFRP strip. Subsequently, analytical models to predict the bond behaviour of modern masonry-to-FRP were developed. However, the advances in the clay brick manufacturing process such us the firing temperature, the use of chemical additives and stricter in place quality controls change the physical and mechanical properties of clay brick masonry when compared to clay bricks manufactured using traditional manufacturing processes approximately 100 years ago [20]. Hence, applicability of the developed models to the bond formed between NSM FRP and vintage clay brick masonry requires further validation.

The strength of the FRP-to-masonry bond depends on the following parameters [10]: the groove and the strip dimensions (see Figure 1), the tensile and shear strength of masonry and groove filler, the level of preparation of the groove substrate and the position of the FRP strip within the member being strengthened. Previously conducted research was undertaken using a variety of test setups, with the most common procedures including small-scale simple block pull tests [10, 21], beam tests [15, 22] and full scale walls loaded out-of-plane [7, 12]. Although beam tests and full scale wall tests are typically considered to provide better representation of how the IC debonding mechanism develops during an earthquake, these test methods are both time consuming and expensive to prepare and undertake. Previous small-scale experimental pull tests considering the FRP to masonry bond behaviour [9, 17-19] included a limited range of brick strength (brick modulus of rupture strength ranging from 3.41 MPa to 3.57 MPa) and a limited variation of geometric parameters, and therefore further research is warranted.

A companion study to the research conducted by Petersen et al. [9], Willis et al. [18] and Kashyap et al. [17] is reported here, that entailed the use of small-scale monotonic pull tests. This

test method was adopted as it permitted a greater number of tests and a wider range of variables to be considered in comparison to the testing of masonry beams or full-scale walls. As no standard testing procedure currently exists pertaining to the method of testing, a large number of different experimental test setups have previously been adopted by various researchers studying the bond strength of FRP-to-concrete and FRP-to-masonry joints. During previous experimental and numerical studies on the bond strength of FRP-to-concrete joints, it was shown that the variation in test setup used can result in substantial differences in the produced test results [23]. The near-end supported single shear pull test setup appears to be the most popular test setup due to its simplicity and proven reliability [24]. It is recognised that this type of single shear pull test setup, that is near-end supported with the masonry in compression, does not necessarily accurately represent a URM wall loaded out-of-plane, where the zone containing the NSM CFRP strip is in tension. However, due to the simplicity and reliability of this test setup and the ability to make direct comparison to the aforementioned studies previously conducted by other [9, 17, 18] the near-end supported single shear pull test setup was selected for the experimental study reported herein. The experimental study reported here consisted of 39 pull-test prisms and the aim of the experimental study was also to investigate the influence of the brick compressive strength and geometric parameters of the FRP strip and the cut groove on the FRP-to-masonry bond. Also, the aim of the experimental study was to acquire experimental results to allow interrogation of the adequacy of existing bond behavioural models of NSM FRP when bonded to vintage clay brick masonry, with the intention of incorporating the model into design guidelines for the seismic strengthening of multi-leaf (also referred to as 'multi-wythe') clay brick URM building components.

2 EXPERIMENTAL PROGRAM

2.1 Material Characterisation

Six brick types with varying mechanical properties were used in the experimental study. All brick types consisted of solid clay bricks with typical nominal dimensions of 230 × 110 × 75 mm, that were sourced and recycled from historic URM buildings located in various parts of New Zealand, with the details of brick origin and building construction date given in Table 1. The mortar mix used in the construction of the masonry prisms had a 1:2:6 ratio by volume of Portland cement, hydrated lime and sand. A stronger mortar mix was adopted in comparison to that suggested for replicating historic masonry [25] in order to reduce the risk of damage during prism relocation and positioning. The adopted mortar mix is expected to have a minimal effect on the test results due to the relatively small portion of bond area where the mortar joints intersected with the FRP strip in comparison to the bond area associated with intersection between the clay bricks and FRP. Willis et al. [18] found that the contribution of the mortar joints to the FRP-to-masonry bond strength was negligible. However, it is recognised that the pull tests reported by Willis et al. [18] were conducted with the mortar joints being in a compressive stress state due to the nature of test setup used. The tension state of masonry is difficult to replicate in a practical manner for small scale tests. Hence, a full scale companion study was conducted [26] in order to validate the realistic out-of-plane loading condition when the masonry is in the tensile state.

Accurate material properties were established by testing the masonry prism assemblages and their constituent materials. Individual bricks were subjected to the half brick compression (f'_b) test [27] whilst incorporating displacement gauges on either side of the half brick, allowing the brick unit stress-strain relationship to be determined. From this data the brick unit Modulus of Elasticity (E_b) was calculated using the stress-strain ordinates at $0.05f'_b$ and $0.70f'_b$ [20]. The compressive strength of the mortar (f'_j) was obtained through compression testing of 50 mm mortar cubes [28] and the masonry prism compressive strength (f'_m) was determined following ASTM C 1314-03b [29]. Modulus of Rupture (f'_{rup}) tests were also conducted on the bricks [27], with results from the aforementioned tests summarised in Table 1.

Carbon FRP (C)FRP strips and a two-part epoxy based adhesive were used in this experimental study due to their high tensile strength and wide availability. Alternative cement based grouts were not considered in this experimental program due to their reduced tensile strength when compared to two-part epoxy based adhesives [30]. In Table 2 the material properties of the CFRP and the adhesive used in the experimental program, as provided in manufacturers' specifications, are compared to experimentally obtained test values. It is also noted that the rupture strain values obtained for the pull test prism C3-4-15-(6/20) compare well to the experimentally obtained values reported in Table 2.

2.2 Pull test prisms

The experimental study consisted of two stages and the following variables were investigated: (i) bond length of the strip (L_b) as illustrated in Figure 1(a); (ii) geometric properties of the reinforcement CFRP strip (b_p and t_p as shown in Figure 1(b)); (iii) geometric properties of the cut groove (d_f and b_f as shown in Figure 1(b)); (iv) brick strength. Critical bond length (L_e) was initially estimated as 100 times the CFRP strip thickness, t_p [18]. The 1.2 mm thickness of the CFRP strip resulted in the required critical bond length of 120 mm and hence masonry prisms consisting of typically 3 bricks in height (approximately 260 mm). The testing consisted of 39 prisms, with the height of the masonry prisms typically increased to 5 bricks to ensure that the bond length, L_b, was greater when compared to the critical bond length and to allow the bond length to be a variable parameter. Table 3 conveys the details of all pull test prisms, with each prism denoted with the following notation:

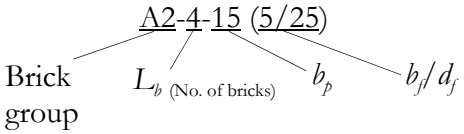

For example, A3-4-15 (5/25) denotes a prism 3 constructed using A group bricks, with a 15 mm wide CFRP strip inserted into a 5 mm × 25 mm groove and bonded to the top four bricks.

2.3 Masonry Prism Preparation

The construction technique for the prisms was kept uniform throughout, with all masonry prisms constructed with a typical mortar joint thickness of approximately 10 mm and the prisms were left to cure at least 28 days prior to installing the bonded CFRP strips. True vertical of the masonry prism with at least one flat face surface (i.e. bricks being in-line to ensure ease of NSM CFRP installation) was achieved by constructing the prisms against a true vertical sideboard as illustrated in Figure 2(a). A centrally located groove was cut into the masonry prism (as depicted in Figure 2(b)) according to the designated dimensions (described previously) using a wet cutting circular saw with a diamond-coated 3 mm thick blade. Installation of CFRP strips was conducted with strict adherence to manufacturer specifications. Once fully dry the groove was cleaned using compressed air and was brushed with acetone to further remove any dust prior to applying adhesive and inserting the CFRP strip.

The CFRP strips were cut into designated dimensions and cleaned with acetone. As reported by Yang [31], strain gauge spacing closer than 50 mm can compromise bond due to the reduced CFRP-masonry bond area. Hence, strain gauges were glued to the strips at spacing of 50 mm, as shown in Figure 3, and positioned equally along the strip with typically a single gauge per brick. Furthermore, strain gauges were attached on alternating sides along the CFRP strip (in comparison to attaching all strain gauges on one side of the CFRP strip only) to reduce the weakening effect on the bond strength.

Two-part epoxy based adhesive was applied both into the groove and directly onto the CFRP strip. The CFRP strip was subsequently inserted into the groove, with the excess epoxy removed. The groove was then completely filled with epoxy until no voids were observed. The CFRP strip was positioned centrally within the groove to a depth that was at least 1 mm less than the total depth of the cut. Following CFRP installation all prisms were left to cure for at least seven days before testing, allowing the epoxy to reach its full strength. To facilitate crack identification, the

front face (i.e. the face containing the CFRP strip) was painted white. The top and bottom of the masonry prism were plastered prior to positioning into the test setup to ensure both a flat resting surface and vertical and horizontal levelling, to minimise eccentricity and to limit bending stresses in the prisms.

2.4 Test setup

Each prism was carefully positioned with the strip centred under the loading grips of the Instron universal testing machine. From preliminary test trials it was established that gripping the CFRP strip directly proved ineffective and slip occurred at loads above approximately 15 kN (on average approximately 30% of the ultimate pull-out loads). To facilitate a greater distribution of stress at the loaded end of the strip a pair of aluminium plates was attached to either side of the CFRP strip using high strength instant adhesive.

End restraints were positioned along each side of the prism's unloaded ends to prevent any lateral movement of the masonry prism. Lu et al. [32], Liu [33] and Seracino et al. [10] observed unrealistic wedge type failure modes when partial end restraint was used. Hence, a full restraint arrangement in the form of a thick solid steel plate with a 40 mm × 15 mm opening was selected, allowing the loading end of the CFRP strip to pass through the opening (see Figure 3). Due to the applied axial force acting eccentrically, significant bending of the prism during a trial testing series was observed. Thus, for the test prisms four steel equal angle sections (25 mm × 25 mm × 3 mm) were used to clamp the prism and reduce the effects of prism bending and rotation, as shown in Figure 4. The steel equal angles were positioned at the prism edges to ensure that the applied stresses due to the support condition were not located within the zone of influence of the CFRP strip.

The test setup consisted of a 10 volts load cell attached to the testing machine to record the applied tensile loading. Instrumentation to record displacement was attached to the CFRP strip

and to the steel restraint plate to record the movement of the CFRP strip relative to the masonry substrate.

3 EXPERIMENTAL RESULTS

3.1 Failure Modes

The observed failure mode and the ultimate failure force, P_{exp}, for each tested prism are presented in Table 3. All prisms that exhibited IC debonding failure developed high shear stresses at the loaded end of the prism, resulting in the formation of herringbone type cracking through the brick in the vicinity of the bonded CFRP strip. The cracks initiated at the top of the prism (loaded end) and with increasing applied axial force propagated down the prism to the unloaded end (see Figure 5). The IC debonding failure mode was further subdivided into two categories: (i) Debonding characterised by the formation of herringbone cracks along the bonded length of the CFRP strip, typically resulting in a trapezoidal failure plane (denoted as H in Table 3) as shown in Figure 6(a); (ii) Debonding characterised by the formation of herringbone cracks along the top part of the prism only and a resulting rectangular failure plane as shown in Figure 6(b) (denoted as R in Table 3; with a combination of the two failure modes denoted H+R as shown in Figure 6(c)).

All observed failures for prisms were sudden and explosive in nature, although visible signs of cracking and plateauing of the force-displacement response at the loaded end (shown in Figure 7) were observed prior to failure. The resulting trapezoidal failure plane for pull test prisms denoted H and H+R was partially attributed to the loading eccentricities in the adopted test setup. As highlighted previously, an attempt was made to rectify the effect of eccentric loading and subsequent rotations of the pull test prisms, leading to a potential trapezoidal failure plane, by using clamped steel equal angels to provide restraint to the test prisms. Based on experimental observations and test results presented here, it is concluded that the crack pattern development

and the observed IC debonding failure planes were similar to those observed in pull-tests with NSM CFRP bonded to concrete substrate (Seracino et al. 2007a), which highlights similarities of the load transfer mechanism for the two construction materials.

The sliding failure mode was observed in 8 prisms. This type of failure mode was typically observed for prisms having thick adhesive layers (df ≥ 9 mm) and for prisms with evidence of poor adhesive bond to CFRP strips observed following testing. Due to under-utilisation of adhesive material and the absence of failure warning signs, sliding failure is deemed undesirable and should be avoided. The sliding failure mode is eluded by not using wide grooves and by ensuring adequate preparation and cleaning of all bonded surfaces.

A NSM CFRP strip is able to develop higher axial strains in comparison to those developed when using the EB technique due to greater confinement from the substrate material, hence making it possible for rupture failure of the CFRP strip to occur. Rupture failure utilises the CFRP material to the full capacity, but provides no visual warning of failure and hence should be avoided in practical scenarios of masonry strengthening. Rupture failure was observed for prism B10-4-25-(6/30) only.

3.2 Parametric Study of Bond Strength

Strip width

Increasing the strip width, with all other variables remaining constant, generally resulted in increased P_{exp} as shown in Figure 8(a). Increasing the strip width by 50% (i.e. from 10 mm to 15 mm) resulted in a 60% increase in ultimate pull-out force. Increasing the strip width by a further 33% (i.e. to 20 mm) resulted in a 13% increase in ultimate pull-out force. Further incremental increases of the strip width by 25% and 20% (i.e. to 25 mm and 30 mm) resulted in a 4% increase and a 10% decrease in ultimate pull-out force respectively.

Masonry prisms strengthened using a 30 mm wide CFRP strip had a tendency to split fully in half at failure. The split occurred at the location of the CFRP strip, resulting in the loss of strip confinement, premature failure, and a subsequent decrease in load carrying capacity, and was attributed to the narrow size of the prism (depth of groove cut being approximately one third of a typically 110 mm wide brick). The premature failure and reduction in load carrying capacity of masonry prisms strengthened using a 30 mm wide CFRP strip contradicts the observations made by Seracino et al. [10] for concrete specimens, where the pull-out capacity increased at a higher rate with increasing strip width due to greater confinement. However, it must be noted that the depth of the groove cut was approximately 7% of the total specimen thickness for the tests reported by Seracino et al. [10] in comparison to the depth of groove cut being approximately 30% of the prism thickness for the study reported here. Also, observations made by Seracino et al. [10] suggest a trapezoidal (H) type failure plane in prisms strengthened using 20 mm wide strips in comparison to rectangular (R) type failure for 10 mm and 15 mm wide CFRP strips. No such correlation between the strip width and the type of failure planes (i.e. rectangular (R) or trapezoidal (H)) can be made for masonry prisms tested as part of the experimental study presented here.

Groove dimensions

The effect of the groove geometry on FRP to masonry bond was investigated as part of the experimental program. The geometry of the CFRP strip remained constant and the groove width, b_f was increased from 3 mm to 12 mm in 3 mm increments. Based on the experimental results, increasing groove width, b_f had no influence on the ultimate applied pull-out axial force. Prisms with groove thicknesses of 9 mm and 12 mm exhibited a sliding failure within the adhesive layer with no decrease in the ultimate axial pull-out force when compared to prisms with a narrower groove width.

Increasing the depth of the groove, d_f with CFRP strip geometry remaining constant did not result in increased ultimate pull-out capacity and hence led to under-utilisation of adhesive material and the initiation of premature brick splitting. As a result, it is recommended that the groove depth be no greater than is required to accommodate the CFRP strip and that at least 5 mm of adhesive cover be provided for minimal protection of the CFRP strip from fire, vandalism and exposure to environmental elements.

Brick strength

Increased brick strength with all other variables remaining constant generally resulted in increased P_{exp}. From Figure 8(b) it is evident that the brick modulus of rupture versus experimental axial force provided a linear fit with an R-squared value of 0.82 in comparison to an R-squared value for the brick compression strength versus experimental axial force of 0.58. As the herringbone crack formation in a direction perpendicular to the principal tensile stress is an indication that the ultimate failure force is related to the brick tensile strength, a linear fit of the experimental results to the brick modulus of rupture is expected.

Bond length

Experimental tests were conducted where all variables were held constant except for the bonded length, L_b of the CFRP strip. As shown in Figure 8(a) (prisms 21, 24, 26, 27 and the average of 6 and 7), P_{exp} did not significantly increase when the critical bond length, L_e was reached. It was found that the critical bond length, L_e was equal to the height of the prism, consisting of either n_b = 3 or 4 bricks.

3.3 Bond Interface Behaviour

All experimentally tested prisms had similar load-slip response at the loaded end, with the representative response for 3 prisms shown in Figure 7. Increasing applied axial tension in the CFRP strip resulted in an increase of the axial strain along the CFRP strip. Two representative examples of strain distribution along the CFRP strip with increased axial force are presented in

Figure 9. For prism B1-4-15-(6/20) (see Figure 9(a)) at maximum loading the strain plateaued at approximatly 13,500 με (80% of the rupture strain specified by the manufacturer). Similar behaviour was observed for prism C6-4-15×2-(6/20) (see Figure 9(c)) with lower axial strain due to the use of 2.4 mm thick CFRP strips.

The shear stress transferred from the CFRP strip to the brick substrate was calcultaed based on strain guage data using Eq. (1).

$$\tau_{avg} = \frac{(\Delta\varepsilon)E_p b_p t_p}{(\Delta L)(2b_p + t_p)} \quad (1)$$

where ΔL = distance between strain gauges; τ_{avg} = average shear stress over the length ΔL; $\Delta\varepsilon$ = change in strain over length ΔL; E_p = modulus of elasticity of FRP strip; b_p = width of the CFRP strip; and t_p = thickness of the CFRP strip. Figure 9(b) and (d) show a typical shear stress distribution along the bonded length with increasing increments of axial tensile strip force for prism B1-4-15-(6/20) (typical) and prism C6-4-15×2-(6/20). As expected, with increasing crack propagation the shear stress distribution (the region of masonry effective in shear transfer) shifted away from the loaded end of the CFRP strip.

The local bond-slip response of the CFRP strip relative to the masonry substrate was determined based on the strain gauge data using a trapezoidal rule method to evaluate the integral of the strain distributions along the bonded length of the CFRP strip. The calculations were based on the assumption that the axial strain in masonry and the slip at the unloaded end could be neglected. It is noted that no slip measurements were made at the unloaded end of the pull test prisms due to limitations in equipment available at the testing laboratory. Note that the assumptions that the axial strain in the masonry and the slip at the unloaded end were negligible and consistent with assumptions previously reported by other researchers [17]. The local bond-slip response derived based on the readings obtained from the first three strain gauges from the loaded end for prism B1-4-15-(6/20) is illustrated in Figure 10. The variation of the local bond-

slip response was observed in all prisms instrumented with strain gauges, with the local bond-slip response typically decreasing with increasing distance towards the unloaded end of the CFRP strip. This variation was partially attributed to the inability of the data logging equipment to record the rapid change in strain that occurred once the cracking had propagated well into the top 2-3 bricks and immediately prior to sudden explosive failure. The variation in the local bond-slip response within the top portion of the bonded length (i.e. top three strain gauges) was insignificant for all prisms and was attributed to the slight variation in strain gauge spacing and the local variation in brick tensile strength and/or location of crack formation. Based on local bond-slip response for all prisms instrumented with strain gauges, three stages for the load transfer mechanism (i.e. elastic, microcracking and macrockracking) for NSM FRP bonded to concrete, as suggested by Yuan et al. [34], are also applicable to vintage clay brick masonry. These stages are defined in Figure 10 for the experimentally obtained local-slip versus shear stress response. The average maximum shear stress for prisms B1-4-15-(6/20), C6-4-15×2-(6/20) and B15-4-15×2-(7/20) was 12.7 MPa, 11.9 MPa and 10.5 MPa respectively.

3.4 Predictive Models

The behaviour of bond between FRP and concrete has been previously studied in substantial detail, resulting in numerous experimental and theoretical data, and published textbooks by Teng et al. [35] and Oehlers and Seracino [36]. From current literature, numerous models are available that are specific for EB FRP bonded to concrete and are well reviewed by Smith and Teng [37], Lu et al. [32], Karbhari et al. [38] and Sayed-Ahmed et al. [39]. Specific analytical models developed for the response of the NSM retrofit technique are reported by Blaschko [21], Hassan and Rizkalla [15] and Seracino et al. [10, 16]. Models proposed by Bleshenko [21] (considering adhesive properties only) and Hassan and Rizkalla [15] (pure shear stress state of concrete assumed) are limited only to the failure modes observed by the authors and are not always consistent with failure modes observed in other experimental tests [9, 10, 17, 18].

The model developed by Seracino et al. [16] is the first published model that is used to predict the IC debonding capacity, P_{IC} (Eq. 2), of both EB and NSM adhesively bonded plates. The IC debonding failure plane aspect ratio, φ_f, and the perimeter of the debonding failure plane cross-section, L_{per}, are given by Eq. (4) and (5), where d_f and b_f are the lengths of the failure plane perpendicular and parallel to the substrate (Figure 1(b)), respectively. Expressions for the maximum interface shear stress, τ_{max}, and the maximum slip, δ_{max}, in the local bond-slip relationship are given by Eq. (6) and (7) respectively, where f_c is the cylinder compressive strength of concrete.

$$P_{IC} = \sqrt{\tau_{max}\delta_{max}}\sqrt{L_{per}(EA)_p} \tag{2}$$

$$\tau_{max}\delta_{max} = C\varphi_f^m f_c^n \tag{3}$$

$$\varphi_f = \frac{d_f}{b_f} \tag{4}$$

$$L_{per} = 2d_f + b_f \tag{5}$$

Based on experimental results and a nonlinear statistical analysis conducted by Seracino et al. [16] the following expressions were obtained:

$$\tau_{max} = (0.802 + 0.078\varphi_f)f_c^{0.6} \tag{6}$$

$$\delta_{max} = \frac{0.976\varphi_f^{0.526}}{0.802 + 0.078\varphi_f} \tag{7}$$

Hence, $P_{IC} = 0.988\varphi_f^{0.263} f_c^{0.3}\sqrt{L_{per}(EA)_p}$ (8)

In an attempt to predict the experimental data reported in Table 3, focus was given to adapting the existing model initially developed by Seracino et al. [16] for predicting the IC debonding capacity, P_{IC}, for both EB and NSM FRP bonded to concrete substrate for application to vintage clay brick masonry. The model was modified by Willis et al. [18] to accommodate the brick

modulus of rupture, f_{ut} (Eq. 9) and was later further modified by Kashyap et al. [17] to incorporate results from a larger experimental database consisting of 137 tests (EB and NSM) of which 34 tests (24.8%) were NSM FRP bonded to modern clay masonry and 2 tests were NSM FRP bonded to concrete masonry [17].

The accuracy of the following model variations and a proposed variation of the existing model for predicting the ultimate pull-out capacity for the experimentally tested prisms reported in Table 3 was assessed:

1. The original Seracino et al. [16] (Eq. 8);
2. The Willis et al. [18] model (Eq. 10), which is obtained by substituting Eq. (9) into Eq. (8) to obtain the relationship for IC debonding resistance presented in Eq. (10);

$$\sqrt{f_c'} = \frac{f_{ut}}{0.53} \tag{9}$$

$$P_{IC} = 1.45\varphi_f^{0.263} f_{ut}^{0.6} \sqrt{L_{per}(EA)_p} \tag{10}$$

3. The Kashyap et al. [17] model for both EB and NSM (Eq. 11);

$$P_{IC} = 2.09\varphi_f^{0.2} f_{ut}^{0.43} \sqrt{L_{per}(EA)_p} \tag{11}$$

4. The Kashyap et al. [17] model for NSM FRP bonded to masonry (Eq. 12);

$$P_{IC} = 2.63\varphi_f^{-0.14} f_{ut}^{0.50} \sqrt{L_{per}(EA)_p} \tag{12}$$

5. The proposed variation of existing model detailed below.

3.5 Variation of Existing Model

Currently available FRP-to-masonry bond models incorporate the brick modulus of rupture as the input parameter for the strength of the substrate material. However, brick and mortar compressive strength is a constituent material parameter that is commonly required as part of the

seismic assessment of historic URM buildings. Hence, the brick compressive strength is commonly assessed as part of the on-site building investigation and material characterisation, and is typically obtained using non-destructive methods or by extracting brick and mortar samples and testing in a laboratory. The compressive strength of clay brick units is hence more readily available than is the brick modulus of rupture, and is more widely used in engineering practice.

In order to provide a simplified FRP-to-masonry bond model that is expressed in terms of brick compressive strength, the relationship between concrete tensile strength and concrete cylinder compressive strength (Eq. 9) proposed by McGregor [40] was compared to an alternative model proposed by Lumantarna et al. [20] and reproduced below as Eq. (13). Experimental results obtained from testing vintage clay bricks [20] are plotted alongside both proposed models in Figure 11. It is evident that the model presented by Lumantarna et al. [20] for solid clay vintage bricks provides an improved correlation with experimental data in comparison to the model suggested by McGregor [40].

$$f_b' = \frac{f_{rup}'}{0.12} \tag{13}$$

Based on the above a modified model in terms of f_b' that incorporates Eq. (12) and Eq. (13) is proposed in Eq. (14).

$$P_{IC} = \frac{\sqrt{f_b' L_{per} (EA)_p}}{\varphi_f^{0.15}} \tag{14}$$

Variations of the Seracino et al. [16] model have each been assessed against obtained experimental results, with the statistical analysis of the experimental-to-predicted strength ratio for each model variation presented in Table 4. Prisms exhibiting a sliding or rupture failure mode, as well as prisms where brick splitting was observed, were excluded from the statistical analysis. The experimental-to-predicted ratio results are compared graphically in Figure 12(a). From Table 4 and Figure 12(a) it is evident that all model variations are generally in good agreement with experimental results. The proposed variation of existing model and the NSM

model by Kashyap et al. [17] both resulted in mean values close to unity, being 1.026 and 0.979 respectively. These two models also had the smallest CoV of 11.4% and 11.5% respectively when compared to the other models considered in Table 4. The generic model proposed by Kashyap et al. [17] resulted in the worst mean value of 0.774 and a CoV of 14.1% which was partially attributed to the large number of specimens having EB FRP that was incorporated within the dataset used for the development of the model. It was concluded that the proposed variation of existing model for predicting the pull-out capacity of NSM CFRP strips in vintage masonry has sufficient accuracy when compared to the obtained experimental results (see Figure 12(b)) with a low CoV (11.4%).

4 BOUNDS OF THE PROPOSED VARAITION OF EXISTING MODEL

The proposed variation of existing model is applicable to the bond of CFRP FRP to vintage clay brick masonry within the bounds of the investigated variables. However, the range of variables investigated and reported here covers a wide range of practical applications (8.9 MPa $\leq f'_b \leq$ 35.8 MPa, 10 mm $\leq b_p \leq$ 30 mm, 1.2 mm $\leq t_p \leq$ 2.4 mm). The IC debonding capacity is limited by the rupture strength of the CFRP strip. Also, in the development of the proposed variation of existing model the prisms that exhibited sliding failure and brick splitting were excluded. However, it must be noted that brick splitting for a strip width of 30 mm and for deeply cut grooves is assumed to be limited in full scale multi-leaf walls where the continuity of the wall provides lateral restraint.

5 CONCLUSIONS

An experimental study was presented that consisted of 39 clay brick prisms that were tested to investigate the behaviour of NSM CFRP strips bonded to vintage solid clay brick masonry. The following can be concluded from the study:

- The main failure mode of the prisms was IC debonding with only 8 prisms exhibiting a sliding type of failure and 1 prism exhibiting rupture failure of the CFRP;
- Masonry prisms strengthened using 30 mm wide CFRP strips had a tendency to split fully in half at failure. The splitting was attributed to the large depth of the groove cut, being approximately 30% of the prism thickness;
- The bond behaviour and load transfer mechanism of CFRP-to-vintage clay brick masonry were found to be similar to CFRP bonded to modern clay brick masonry and CFRP bonded to concrete;
- Severe bending of the prisms was observed due to eccentrically applied force in cases where laterally unrestrained prisms were tested (trail tests), resulting in low pull-out forces;
- Analytical models currently available in the literature were assessed using the available experimental results and a modified variation of existing model was proposed. For the range of experimental parameters included as part of the study reported here, the predicted values from the proposed variation of existing model correlated well with the experimentally obtained results;
- The proposed variation of the existing analytical model is rather simple but provides a straightforward approach for a practicing structural engineer to evaluate the pull-out resistance of NSM FRP strips using readily available mechanical properties of building constituent materials.

6 ACKNOWLEDGEMENTS

The authors wish to thank and acknowledge the support provided by the technical staff of the Department of Civil and Environmental Engineering at the University of Auckland. The authors also thank Contech Limited and Sika NZ for supplying the CFRP and epoxy used in this

research. This study was conducted with financial support provided by the New Zealand Foundation for Research, Science and Technology (FRST).

7 REFERENCES

[1] Gledhill K, Ristau J, Reyners M, Fry B, Holden C. The Darfield (Canterbury) earthquake of September 2010: Preliminary seismological report. Bulletin of the New Zealand Society for Earthquake Engineering. 2010;43:215-21.

[2] Bradley BA, Cubrinovski M. Near-Source Strong Ground Motion Observated in the 22 Febuary 2011 Christchurch Earthquake. Bulletin of New Zealand Society for Earthquake Engineering. 2011;44:181-95.

[3] Ingham JM, Griffith MC. Performance of unreinforced masonry buildings during the 2010 Darfield (Christchurch, NZ) earthquake. Australian Journal of Structural Engineering. 2011;11:207-24.

[4] Dizhur D, Ingham JM, Moon L, Griffith MC, Schultz A, Senaldi I et al. Performance of masonry buildings and churches in the 22 February 2011 Christchurch earthquake. Bulletin of New Zealand Society for Earthquake Engineering. 2011;44:279-97.

[5] Dizhur D, Ismail N, Knox C, Lumantarna R, Ingham JM. Performance of unreinforced and retrofitted masonry buildings during the 2010 Darfield earthquake. Bulletin of the New Zealand Society for Earthquake Engineering. 2010;43:321-39.

[6] Griffith MC, Magenes G, Melis G, Picchi L. Evaluation of out-of-plane stability of unreinforced masonry walls subjected to seismic excitation. Journal of Earthquake Engineering. 2003;7:141-69.

[7] Korany Y, Drysdale R. Rehabilitation of masonry walls using unobtrusive FRP techniques for enhanced out-of-plane seismic resistance. Journal of Composites for Construction. 2006;10:213-22.

[8] Mosallam AS. Out-of-plane flexural behavior of unreinforced red brick walls strengthened with FRP composites. Composites Part B: Engineering. 2007;38:559-74.

[9] Petersen RB, Masia MJ, Seracino R. Bond Behavior of Near-Surface Mounted FRP Strips Bonded to Modern Clay Brick Masonry Prisms: Influence of Strip Orientation and Compression Perpendicular to the Strip. Journal of Composites for Construction. 2009;13:169-78.

[10] Seracino R, Jones NM, Ali MSM, Page MW, Oehlers DJ. Bond Strength of Near-Surface Mounted FRP Strip-to-Concrete Joints. Journal of Composites for Construction. 2007;11:401-9.

[11] Derakhshan H, Griffith M, Ingham J. Out-Of-Plane Behavior of One-Way Spanning Unreinforced Masonry Walls. Journal of Engineering Mechanics.0:277.

[12] Willis CR, Yang Q, Seracino R, Griffith MC. Damaged masonry walls in two-way bending retrofitted with vertical FRP strips. Construction and Building Materials. 2009;23:1591-604.

[13] Oehlers DJ, Seracino R. Design of FRP and Steel Plated RC Structures. Oxford: Elsevier Science; 2004. p. 24-45.

[14] Stone D, Tumialan G, Nanni A, Perretti R. Near surface mounted FRP reinforcement: Application of an emerging technology. Concrete International. 2002;35:42-4.

[15] Hassan T, Rizkalla S. Investigation of Bond in Concrete Structures Strengthened with Near Surface Mounted Carbon Fiber Reinforced Polymer Strips. Journal of Composites for Construction. 2003;7:248-57.

[16] Seracino R, Saifulnaz MR, Oehlers DJ. Generic Debonding Resistance of EB and NSM Plate-to-Concrete Joints. Journal of Composites for Construction. 2007;11:62-70.

[17] Kashyap J, C.R. W, Griffith MC, Ingham JM. Debonding Resistance of FRP-to-Masonry Joints. Engineering Structures. 2012;40:186-98.

[18] Willis CR, Yang Q, Seracino R, Griffith MC. Bond behaviour of FRP-to-clay brick masonry joints. Engineering Structures. 2009;31:2580-7.

[19] Konthesingha KMC, Masia MJ, Petersen RB, Page AW. Bond behaviour of NSM FRP strips to modern clay brick masonry prisms under cyclic loading. 11th Canadian Masonry Symposium. Toronto, Canada: McMaster University / Canadian Masonry Design Centre; 2009. p. 665-74.

[20] Lumantarna R, Biggs DT, Ingham JM. Studies on the physical and mechanical properties of vintage solid clay bricks. Journal of Materials and Structures. 2012;under review.

[21] Blaschko M. Bond behaviour of cfrp strips glued into slits. Sixth International Symposium on FRP Reinforcement for Concrete Structures (FRPRCS-6). Singapore2003.

[22] De Lorenzis L, Lundgren K, Rizzo A. Anchorage Length of Near-Surface Mounted Fiber-Reinforced Polymer Bars for Concrete Strengthening - Experimental Investigation and Numerical Modeling. ACI Structural Journal. 2004;101:269-78.

[23] Chen JF, Teng JG. Anchorage strength models for FRP and steel plates bonded to concrete. Journal of Structural Engineering. 2001;127:784-91.

[24] Yao J, Teng JG, Chen JF. Experimental study on FRP-to-concrete bonded joints. Composites Part B: Engineering. 2005;36:99-113.

[25] Dizhur D, Ingham JM. Diagonal tension strength of vintage unreinforced clay brick masonry. Construction and Building Materials. 2012;Under review.

[26] Dizhur D. Performance of masonry buildings in the Canterbury earthquakes and corresponding strengthening solution using NSM CFRP. Doctorate Thesis, The University of Auckland; 2013.

[27] ASTM. Standard Test Methods for Sampling and Testing Brick and Structural Clay Tile C 67-03a. ASTM International. Pennsylvania, United States2003.

[28] ASTM. Standard Test Method for Compressive Strength of Hydraulic Cement Mortars (Using 2-in. or [50-mm] Cube Specimens) C 109/C 109M - 08. ASTM International. Pennsylvania, United States2008.

[29] ASTM. Standard Test Method for Compressive Strength of Masonry Prisms. C 1314-03b. ASTM International. Pennsylvania, United States.2003.

[30] Täljsten B, Carolin A, Nordin H. Concrete structures strengthened with near surface mounted reinforcement of CFRP. Advances in Structural Engineering. 2003;6:201-13.

[31] Yang Q. Seismic retrofit of URM walls with externaly bonded FRP composites. Adelaide: The Univeristy of Adelaide; 2006.

[32] Lu XZ, Teng JG, Ye LP, Jiang JJ. Bond-slip models for FRP sheets/plates bonded to concrete. Engineering Structures. 2005;27:920-37.

[33] Liu I. Retrofitting reinforced concrete beams and slabs by adhesively bonding new advanced fibre reinforced polymer (FRP) composites to their surface. Adelaide, Australia The University of Adelaide; 2005.

[34] Yuan H, Teng JG, Seracino R, Wu ZS, Yao J. Full-range behavior of FRP-to-concrete bonded joints. Engineering Structures. 2004;26:553-65.

[35] Teng JG, Chen JF, Smith ST, Lam L. FRP Strengthened RC Structures Chichester, England: John Wiley and Sons Limited 2002.

[36] Oehlers DJ, Seracino R. Design of FRP and Steel Plated RC Structures: Retrofitting of Beams and Slabs for Strength, Stiffness and Ductility. Elservier, Kinlington, Oxford, UK2004.

[37] Smith ST, Teng JG. FRP-strengthened RC beams. II: Assessment of debonding strength models. Engineering Structures. 2002;24:397-417.

[38] Karbhari VM, Niu H, Sikorsky C. Review and comparison of fracture mechanics-based bond strength models for FRP-strengthened structures. Journal of Reinforced Plastics and Composites. 2006;25:1757-94.

[39] Sayed-Ahmed EY, Bakay R, Shrive NG. Bond strength of FRP laminates to concrete: State-of-the-art review. Electronic Journal of Structural Engineering. 2009;9:45-61.

[40] MacGregor JG. Reinforeced concrete: Mechanics and design. New Jersey: Prentice Hall: Englewood Cliffs; 1988.

[41] DIN53455. Testing of Plastics; Tensile Test. Berlin: Deutsches Institut für Normung (DIN) 1981.

[42] EN196-1. Methods of testing cement - Part 1: Determination of strength. Brussels: European Committe for Standardization; 2005.

[43] ASTM. Standard Test Method for Compressive Properties of Rigid Plastics D695 - 10. Pennsylvania, United States.: ASTM International 2010.

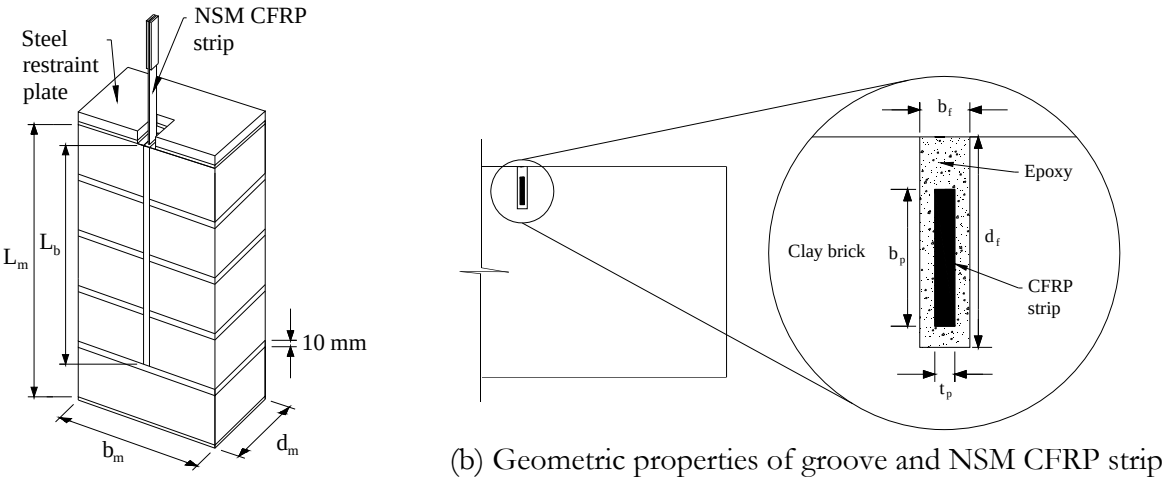

(a) Geometric properties of the masonry prism

(b) Geometric properties of groove and NSM CFRP strip

Figure 1: Prism geometrical detailing

(a) Masonry prism construction against sideboard

(b) Groove cutting

Figure 2: Prism construction details

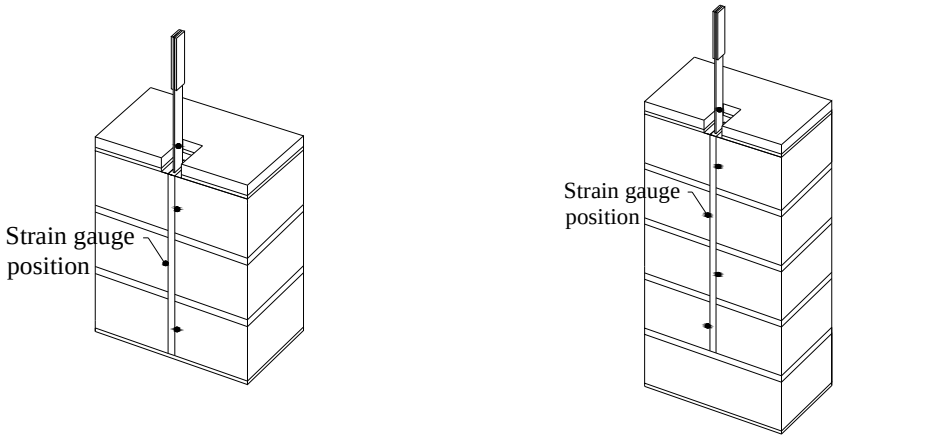

(a) Typical position of strain gauges (three brick prism)

(b) Typical position of strain gauges (five brick prism)

Figure 3: Position of strain gauges

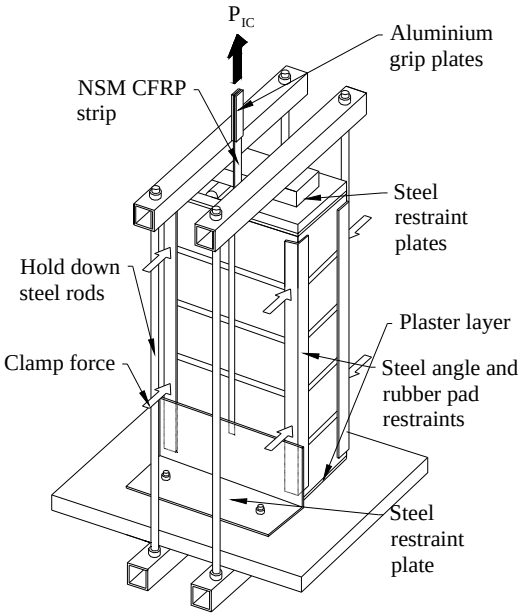

Figure 4: Typical pull test setup

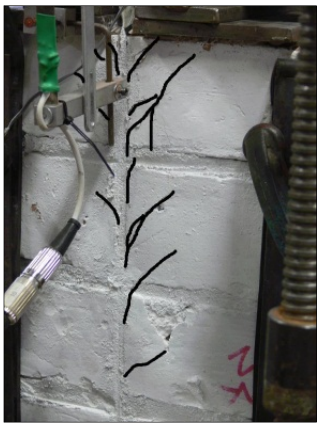

(a) Initiation of herringbone cracks D2-4-15-(7/20)

(b) Top view of prism following failure B1-4-15-(6/20)

Figure 5: Crack pattern

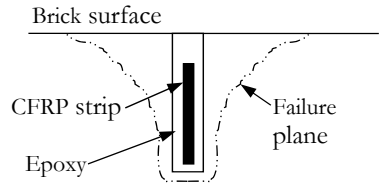

(a) Trapezoidal failure plane, H F2-4-15-(6/20)

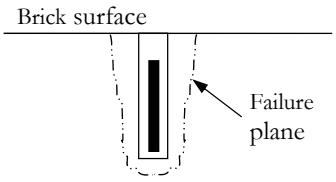

(b) Rectangular failure plane, R C2-4-25-(6/30)

(c) Trapezoidal and rectangular failure plane, H+R E1-4-15-(6/20)

Figure 6: IC debonding failure planes

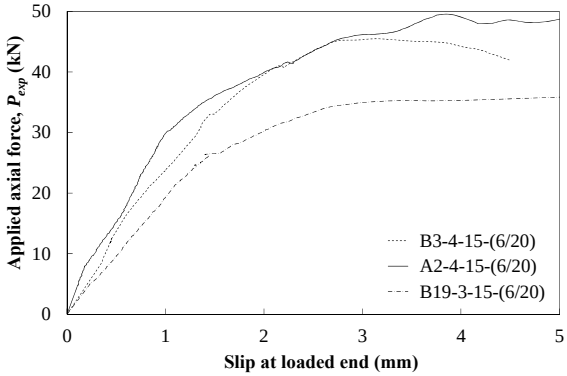

Figure 7: Typical load-slip response

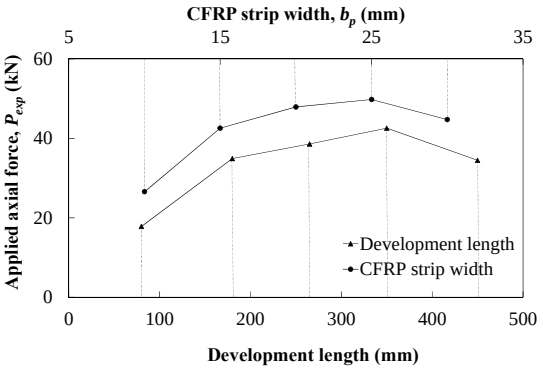

(a) Effect of development length and strip width on pull-out strength

(Development length prisms plotted: 21, 24, 26, 27, and the average of 6 and 7; CFRP strip width prisms plotted: 14, 15, 16, the average of 7 and 12, and the average of 12 and 13)

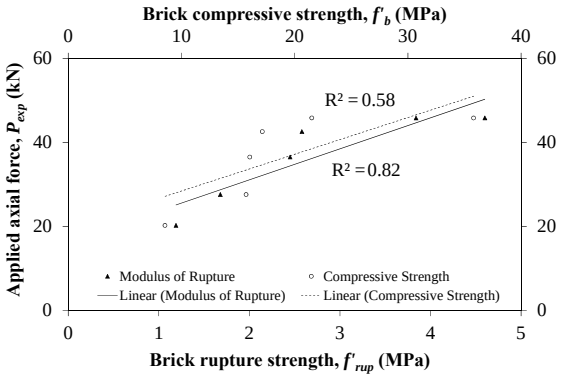

(b) Effect of brick compressive and rupture strength on pull-out strength

Figure 8: Effects of variables on bond strength

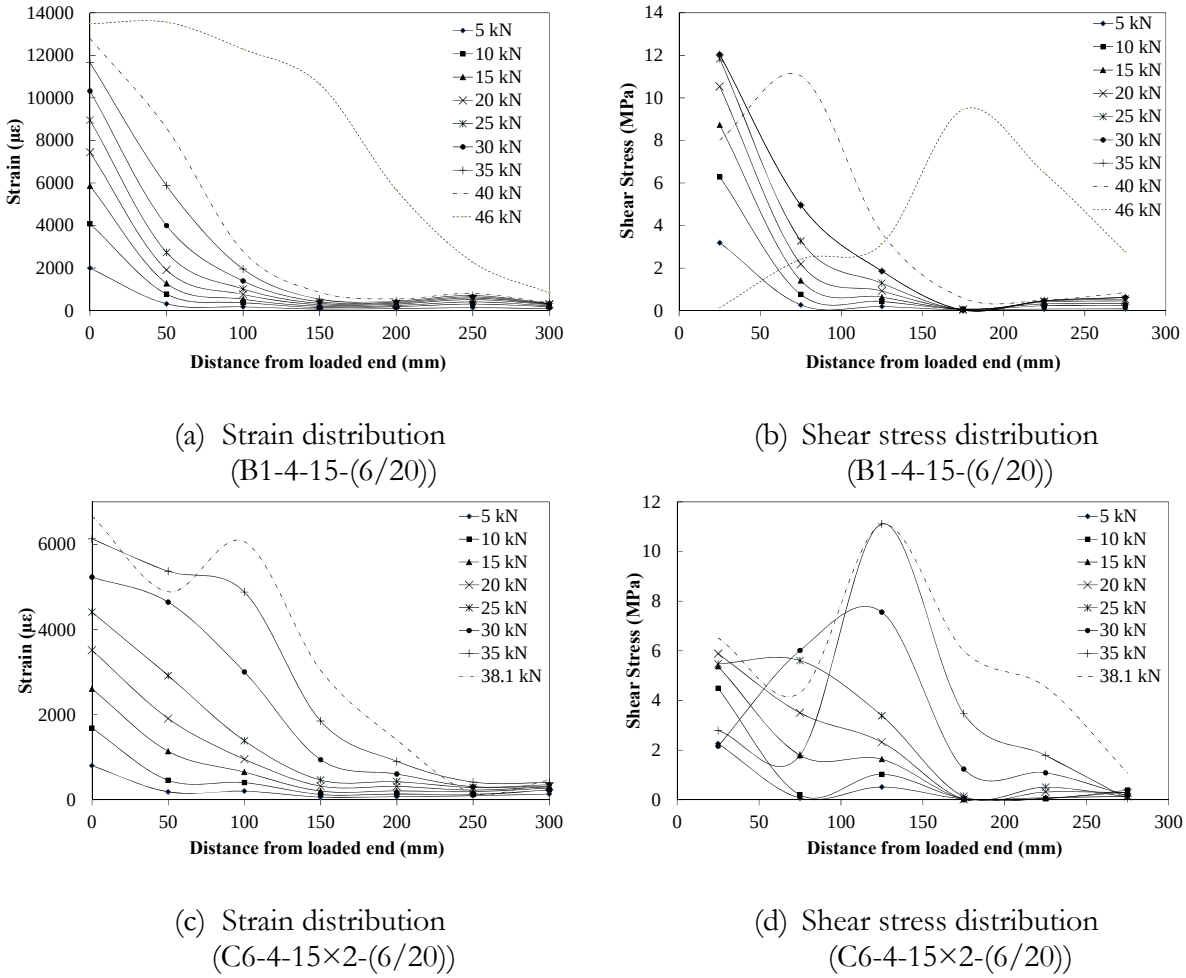

(a) Strain distribution (B1-4-15-(6/20))

(b) Shear stress distribution (B1-4-15-(6/20))

(c) Strain distribution (C6-4-15×2-(6/20))

(d) Shear stress distribution (C6-4-15×2-(6/20))

Figure 9: Typical experimental results

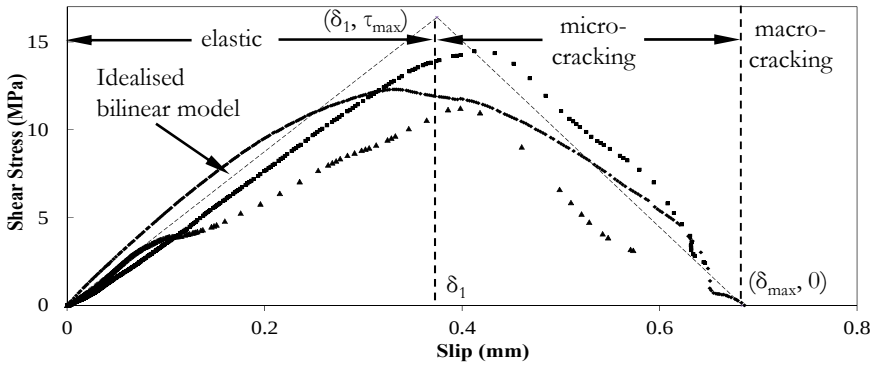

Figure 10: Local bond-slip curve for B1-4-15-(6/20) prism (first three strain gauges)

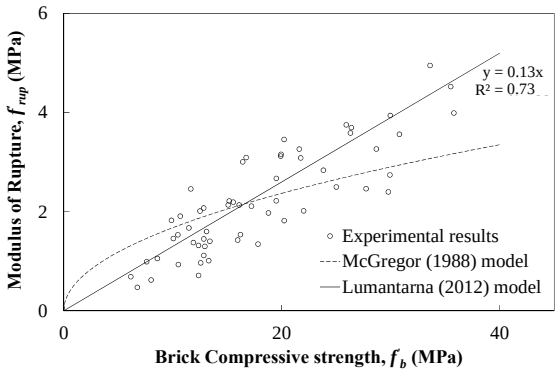

Figure 11: Brick compressive strength vs. modulus of rupture

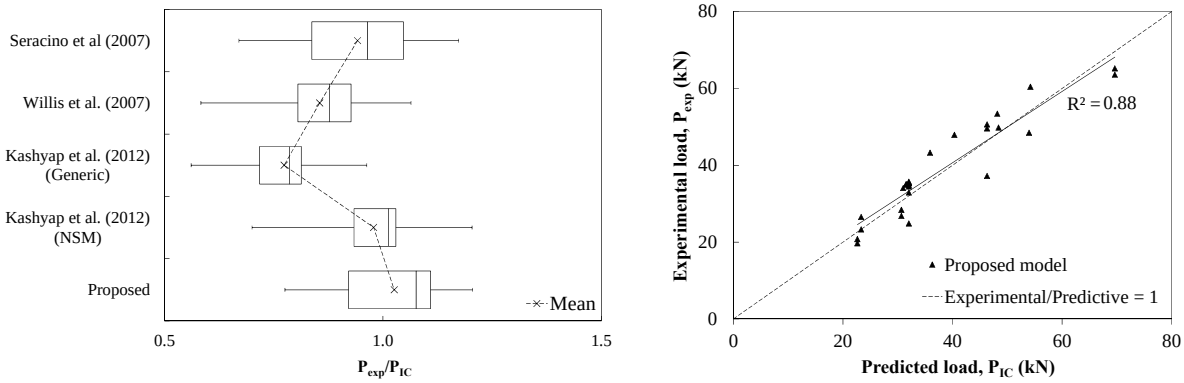

(a) Statistical comparison of available predictive FRP to masonry bond

(b) Experimental against predicted loading

Figure 12: Experimental-to-predicted ultimate pull-out force comparison

Table 1: Masonry material properties

Brick group	Origin & year built	f'_b (N/mm²)	n	f'_m (N/mm²)	n	f'_j (N/mm²)	n	f'_{rup} (N/mm²)	n	E_b (N/mm²)	n
A	Auckland, 1930's	35.8 (0.21)	10	-				3.8 (0.14)	8	9,600 (0.35)	6
B	Auckland, 1940's	17.1 (0.15)	10	7.79 (0.14)	3			2.6 (0.26)	11	6,200 (0.29)	4
C	Auckland, pre-1930's	21.5 (0.25)	8	-		15.0 (0.11)	6	3.4 (0.24)	9	3,600 (0.42)	5
D	Auckland, 1910	16.0 (0.11)	6	-				2.5 (0.35)	4	3,000 (0.38)	10
E	Gisborne, 1906	15.7 (0.21)	8	-				1.9 (0.36)	9	2,700 (0.32)	10
F	Wellington, 1884	8.9 (0.18)	9	-				1.2 (0.29)	5	1,000 (0.47)	9

Note: n – sample size; ( ) – coefficient of variation (CoV).

Table 2: CFRP and adhesive material data

Property	Adhesive			CFRP		
	Manufacture's specifications	Experimental results	n	Manufacture's specifications	Experimental results	n
Compressive strength (N/mm²)	90.0 [EN 196-1]	82.5 (0.13)	5	-	-	-
Shear strength (N/mm²)	17.5 [FIP 5.15]	N/A	-	-	-	-
Tensile strength (N/mm²)	28.5 [DIN 53455]	N/A	-	3,100	2,850 (0.23)	3
Modulus of elasticity, E (N/mm²)	9,600 [ASTM D695]	N/A	-	165,000	155,00 (0.11)	3
Rupture strain, ε_{rup} (με)	-	-	-	17,000	12,200	3

Note: [ ] - signifies testing standard used from manufacture's provided literature; N/A – data not available; ( ) – coefficient of variation (CoV); n – sample size.

Table 3: Geometric details and experimental results of pull-out prisms

Test #	Prism name	Prism parameters			Retrofit parameters					Experimental results		
		Brick group	L_m (mm)	b_m (mm)	t_p (mm)	b_p (mm)	b_f (mm)	d_f (mm)	L_b (mm)	P_{exp} (kN)	Failure mode	Prism splitting
1	A1-4-15-(6/20)	A	430	110	1.2	15	6	20	320	37.2	H	N
2	A2-4-15-(6/20)		420	105	1.2				315	49.6	R	
3	A3-4-15-(6/20)		425	120	1.2				325	50.6	R	
4	A4-4-15×2-(6/20)		435	115	2.4				310	60.6	H+R	
5	A5-4-15×2-(6/20)		420	110	2.4				315	65.2	H+R	
6	B1-4-15-(6/20)	B	435	105	1.2				360	47.2	H+R	
7	B2-4-15-(7/20)		450		1.2		7		340	40.0	H+R	
8	B3-4-15-(6/20)		440		1.2		6		350	45.6	S	
9	B4-4-15-(3/20)		450		1.2		3		350	35.1	H	
10	B5-4-15-(9/20)		450		1.2		9		360	43.1	S	
11	B6-4-15-(12/20)		435		1.2		12		350	35.7	H	
12	B7-4-10-(6/15)		445		1.2	10	6	15	350	23.3	H	
13	B8-4-10-(6/15)		445		1.2		6		350	26.6	H+R	
14	B9-4-20-(7/25)		450		1.2	20	7	25	360	41.9	H	
15	B10-4-25-(6/30)		445		1.2	25	6	30	380	49.8	H	
16	B11-4-30-(6/35)		450		1.2	30		35	360	37.3	S	
17	B12-4-15-(6/25)		435		1.2	15		25	350	46.3	S	
18	B13-4-15-(6/30)		450		1.2			30	360	32.9	H	
19	B14-4-15-(6/35)		450		1.2			35	360	35.5	H	
20	B15-4-15×2-(7/20)		440		2.4		7		360	53.4	H	
21	B16-5-15-(6/20)		450		1.2		6		450	34.5	H	
22	B17-4-15-(6/25)		435		1.2			25	350	24.9	H	
23	B18-4-30-(6/35)		430		1.2	30		35	360	44.7	H+R	
24	B19-3-15-(6/20)		265		1.2	15		20	265	38.6	H	
25	B20-3-30-(6/20)		260		1.2	10		20	260	25.2	H+R	
26	B21-2-15-(6/20)		170		1.2	15		20	180	34.9	H+R	
27	B22-1-20-(6/20)		80		1.2	20		20	80	17.8	H	
28	C1-4-10-(6/15)	C	390	110	1.2	10	6	15	310	33.0	S	N
29	C2-4-25-(6/30)				1.2	25		30	310	60.4	R	
30	C3-4-15-(6/20)				1.2	15		20	310	46.1	Rupture	
31	C4-4-15-(6/20)				1.2	15		20	310	48.2	S	
32	C5-4-15-(6/20)				1.2	15		20	310	43.3	H	
33	C6-4-15×2-(6/20)				2.4	15		20	310	48.5	H	
34	D1-4-15-(6/20)	D	455	120	1.2	15	6	20	350	39.0	S	N
35	D2-4-15-(7/20)		460				7			34.1	H+R	
36	E1-4-15-(6/20)	E	420	110	1.2	15	6	20	330	28.4	H+R	Y
37	E2-4-15-(6/20)		425							26.8	S	N
38	F1-4-15-(6/20)	F	415		1.2	15	6	20	330	20.8	H	N
39	F2-4-15-(6/20)		420							19.7	H	

Table 4: Comparison of experimental-to-predicted strength ratio

Model	Mean	Median	Max	Min	SD	COV
Proposed	1.03	1.08	1.21	0.78	0.18	0.11
Kashyap et al. [17] NSM	0.98	1.01	1.20	0.70	0.11	0.12
Kashyap et al. [17] Generic	0.77	0.79	0.96	0.56	0.11	0.14
Willis et al. [18]	0.86	0.88	1.06	0.58	0.12	0.14
Seracino et al. [16]	0.94	0.97	1.17	0.67	0.14	0.15

Note: SD - standard deviation; COV - Coefficient of variation.